Research Square

Preprints are preliminary reports that have not undergone peer review.
They should not be considered conclusive, used to inform clinical practice,
or referenced by the media as validated information.

Uncovering the hidden crustal nature beneath the enormous post-rift sediments in Bangladesh

M. Ismaiel

ismaiel@iitdalumni.com

IISER Pune https://orcid.org/0000-0001-8059-6577

M Rishal

IISER Pune

Article

Keywords: Bangladesh, Bengal Basin, Moho Depth, crustal density, Receiver function, gravity Anomaly

Posted Date: November 24th, 2026

DOI: https://doi.org/10.21203/rs.3.rs-11828888/v1

License: This work is licensed under a Creative Commons Attribution 4.0 International License.
Read Full License

Additional Declarations: There is **NO** Competing Interest.

Uncovering the hidden crustal nature beneath the enormous post-rift sediments in Bangladesh

M. Rishal[1], and M. Ismaiel[1*]

[1]Department of Earth and Climate Science, Indian Institute of Science Education and Research Pune, Pune, 411 008, India

*Correspondence: ismaiel@iitdalumni.com

Abstract:

The crust beneath Bangladesh is buried beneath a 15–20 km-thick sedimentary succession and subducts beneath the Burma Plate along its eastern boundary. Over the past three decades, the nature of crust in this region has been interpreted as either transitional continental crust or oceanic-affinity crust, with important implications for reconstructing the eastern margin of the Indian Plate. Here, we develop an integrated geophysical approach that jointly inverts teleseismic receiver functions and gravity anomalies to constrain crustal thickness and bulk density independently, avoiding reliance on empirical seismic velocity–density relationships. Our results reveal Moho depths of 28 – 34 km across much of the study area, locally decreasing to crustal thicknesses of less than 15 km, and average crust density of 2938 – 2965 kg m^{-3}. The inferred crustal density is more than global continental crust density (2880 kg m^{-3}) which supports the presence of thick crust with oceanic affinity beneath the onshore Bengal Basin. We further compare crustal and sediment thickness variations in western Bangladesh with a non-uniform, magma-assisted rifting model. The model indicates greater lithospheric than crustal thinning (β-ratio > 2), accompanied by magmatic addition to the thinned continental crust. However, the model cannot independently account for the anomalously 12.5 km thick sedimentary deposition. Explaining this excess subsidence and accommodation space may require contributions from dynamic topography (< 1 km), enhanced lower-crustal flow and sediment lithification, acting individually or in combination. These findings provide new constraints on the crustal architecture beneath the Bengal Basin and demonstrate the importance of integrating seismic and gravity observations to investigate crustal modification and anomalous subsidence along magma-rich rifted margins.

Keywords: *Bangladesh, Bengal Basin, Moho Depth, crustal density, Receiver function, gravity Anomaly*

1. Introduction:

Bangladesh is situated within a tectonically active region along the eastern margin of the Indian Plate, where plate convergence, crustal deformation, and the accumulation of thick sedimentary sequences have profoundly influenced its geological evolution (Govin et al., 2018; Kumar et al., 2015; Mallick et al., 2019; Mitchell, 1981; Ni et al., 1989; Steckler et al., 2008; 2024). The Indian Plate, which subducts beneath the Burmese Plate, is deeply buried beneath a 15–20 km-thick sedimentary succession delivered by the Ganges–Brahmaputra river system (Fig. 1, Betka et al., 2018; Khin et al., 2017; Milliman and Farnsworth, 2011; Milliman and Syvitski, 1992; Steckler et al., 2008). The lithosphere beneath Bangladesh experienced continental extension associated with the impingement of the Kerguelen mantle plume at approximately 118 Ma, while the breakup of microcontinents contributed to lithospheric thinning and magmatic modification during the Early Cretaceous (Alam et al., 2003; Kent et al., 2002; Krishna et al., 2022; Talwani et al., 2016). These tectono-magmatic events may have produced a heterogeneous crust comprising stretched continental crust with magmatic additions and potentially oceanic-affinity crust beneath present-day Bangladesh. The thick sedimentary succession obscures the underlying crustal architecture, complicating palaeo-reconstructions of the eastern Indian margin and our understanding of its subsequent evolution under substantial sediment loading and plate convergence (Frielingsdorf et al., 2008; Ismaiel et al., 2019; Steckler et al., 2008; Uddin and Lundberg, 1998).

The nature of the crust beneath Bangladesh has remained debated over the past two decades, with different geophysical investigations suggesting contrasting crustal affinities. A major challenge is the exceptionally thick sedimentary succession, which locally reaches approximately 15–20 km and obscures the underlying crystalline crustal architecture. Several studies have interpreted the region as transitional crust with oceanic affinity (Arora et al., 2024; Mitra et al., 2018; Sadler et al., 2026; Singh et al., 2016; Wang et al., 2019), whereas others have proposed a transitional domain with continental affinity (Sibuet et al., 2016; Rangin & Sibuet, 2017). An oceanic crustal origin, including its offshore continuation, has also been proposed based on gravity and seismic data (Ismaiel et al., 2019; Krishna et al., 2022; Talwani et al., 2016, 2017). These interpretations have regional implications for the nature of the Indian Plate approaching the Indo-Burma subduction system. Seismic investigations in Myanmar suggest the subduction of Indian continental lithosphere (Zheng et al., 2020), whereas a predominantly mafic composition of the subducting crust has also been proposed (Arora et al., 2024). Whether the lithosphere approaching the Indo-Burma subduction zone comprises

thinned continental crust, oceanic crust, or a magmatically modified transitional domain remains an important unresolved problem. Addressing this ambiguity requires improved constraints on crustal structure and the spatial extent of crustal thinning beneath the sediment-covered Bengal Basin.

The crustal thickness beneath Bangladesh and adjacent regions, ranging from approximately 35–45 km beneath the Indian craton to 25–35 km across the Bengal Basin (Arora et al., 2024; Carchedi et al., 2025; Damodara et al., 2017; Mandal, 2022; Mitra et al., 2008, 2018; Krishna et al., 2022; Rajasekhar and Mishra, 2008; Sadler et al., 2026; Singh et al., 2016). These spatial variations in crustal thickness from the Indian craton to the Bengal Basin have been attributed to crustal thinning accompanied by magmatic additions associated with the Rajmahal–Sylhet volcanic activity (Kent et al., 2002; Talwani et al., 2016; Singh et al., 2016). Land gravity data from Bangladesh have also revealed characteristics consistent with a continental-to-oceanic transition beneath the Bengal Basin (Krishna et al., 2022). However, existing observations do not yet provide a robust assessment of the crustal density structure to distinguish between competing models, owing to the non-uniqueness of gravity interpretations and the exceptionally thick sedimentary succession. Apart from this, the relationship between lithospheric extension, magmatic addition and extreme sedimentary basin development in Bangladesh, also remains unresolved.

Here, we perform a joint inversion of teleseismic receiver functions and land gravity data to constrain crustal thickness and density structure beneath Bangladesh. We further compare the observed crustal and sedimentary thickness variations with a non-uniform, magma-assisted rifting model to examine ratio between crustal and lithospheric thinning and magmatic additions. Our results provide new constraints on crustal structure and lithospheric evolution beneath Bangladesh, with implications for the eastern Indian margin and the Indian Plate approaching the Indo-Burma subduction system.

2. Geological and tectonic setting of Bangladesh

Bangladesh is located on the northeastern margin of the Indian Plate, adjacent to actively convergent plate boundaries to the east and north (Fig. 2). The study area is characterized by a low-lying plain underlain by a deeply subsided basin, contrasting with the elevated crystalline basement terrains to the west and the Shillong Plateau to the north (Fig. 1; Tozer et al., 2019). The tectonic evolution of the sedimentary basin in Bangladesh is closely linked to the Early Cretaceous (120–118 Ma) separation of continental fragments from Greater India and plate

reorganizations associated with the Kerguelen mantle plume (Talwani et al., 2016; Asimus et al., 2025). The continental extension phase resulted in a heterogeneous crustal architecture beneath the Bengal Basin and the development of a sedimentary basin along a volcanic rifted margin (Alam et al., 2003; Ismaiel et al., 2019; Krishna et al., 2022; Mitra et al., 2018; Rajasekhar & Mishra, 2008; Singh et al., 2016). The hinge zone constitutes an important structural transition between the western continental domain and the eastern crustal domain of oceanic affinity, with implications for the regional flexural response and subsidence of the basin (Alam et al., 2003).

The basement beneath the Bengal Basin has subsided to a maximum depth of approximately 20 km over the past 120 Ma (Fig. 2b, Curray, 1991; Curray & Moore, 1971; Khan & Chouhan, 1996; Steckler et al., 2016). Seismic investigations reveal substantial lateral variations in sediment thickness and crystalline crustal structure, with total crustal thicknesses of approximately 30–40 km, indicating that only about 15–20 km of crystalline crust remains beneath the deepest parts of the basin after accounting for the sedimentary succession (Singh et al., 2016; Mitra et al., 2018; Wang et al., 2019). The basin's structural and sedimentary evolution has been modified by ongoing plate convergence along its eastern margin, where the Indian Plate has been obliquely subducting beneath the Burma microplate at approximately 40–50 mm/yr since the Middle Miocene (Acharyya, 2007; Bürgi et al., 2021; Hossain et al., 2020; Maurin & Rangin, 2009; Socquet & Pubellier, 2005; Steckler et al., 2008, 2016; Vorobieva et al., 2021; Wang et al., 2014). This convergence has facilitated the formation of a prominent fold-and-thrust belt along the overriding Burma microplate (Fig. 1). Subduction beneath the Surma Basin, involving negatively buoyant transitional oceanic lithosphere since approximately 8–14 Ma, has also been associated with uplift of the Shillong Plateau through displacement along the Dauki Thrust and westward propagation of the Indo-Burman Wedge (Mallick et al., 2019, 2020). The sedimentary evolution of the Surma Basin, south of the Shillong Plateau, has been interpreted as comprising an earlier passive-margin depositional phase until approximately 3.5 Ma, followed by sediment accumulation within a flexurally influenced basin (Najman et al., 2016). Viscoelastic modelling suggests that sediment and ocean loading over the past 18,000 years contribute approximately 1.1–1.6 mm/yr to present-day subsidence (Karpytchev et al., 2018), whereas GNSS observations reveal spatially variable subsidence rates of 3–7 mm/yr, locally exceeding 20 mm/yr in coastal Bangladesh, reflecting the combined effects of deep lithospheric adjustment and shallow sediment compaction (Steckler et al., 2024). The present-day configuration of the Bengal Basin therefore reflects the

interplay between inherited crustal structure, lithospheric extension and thinning, sediment accumulation, and tectonic convergence. Understanding the relative contributions of these processes is essential for constraining the deep crustal architecture and subsidence mechanisms responsible for the development of the 20-km-deep basin.

3. Data and Methods:

3.1 Data: The SRTM15+ elevation dataset was downloaded from the public domain (Tozer et al., 2019) and used to generate the topographic map of the study area (Fig. 1). The total sediment thickness map was prepared using publicly available datasets from the USGS (2001) and Stolk et al. (2013) (Fig. 2b). The onshore Bouguer gravity anomaly data were adopted from the compiled gravity anomaly map of Bangladesh by Krishna et al. (2022), whereas the offshore free-air gravity anomaly data were obtained from Sandwell et al. (2014) (Fig. 3a). The onshore Bouguer and offshore free-air gravity anomalies were referenced to a common datum level. We obtained broadband seismic data from 28 stations of the Bangladesh–India–Myanmar Array (BIMA and XI FDSN network; Fig. 1), covering the period from 2018 to 2022, for receiver function analysis.

3.2 Residual Mantle Gravity Anomaly: The observed gravity anomaly reflects the combined effects of sedimentary density variations, lithospheric thermal structure, and residual mantle anomalies associated with variations in Moho topography and density contrast across the crust–mantle interface. The gravity signal associated with the crust–mantle boundary was isolated by removing the contributions of sedimentary gravity anomalies and lithospheric thermal and pressure effects from the Bouguer gravity anomaly. The residual mantle gravity anomaly was subsequently incorporated into the joint inversion of receiver function and gravity data to constrain Moho depth and the density contrast across the crust–mantle interface (Fig. 3b). A detailed description is provided in the Supporting Information (Text S1).

3.3 Telesesimic receiver functions: Teleseismic: *P*-wave recordings from stations BA and BN were selected for earthquakes with magnitudes of $M \geq 5.5$ and epicentral distances of 30–90° (Figs. 1 and S1). The seismic waveforms were band-pass filtered between 0.05 and 1 Hz, and radial receiver functions were calculated using iterative time-domain deconvolution (Ligorría & Ammon, 1999) with a Gaussian factor of 2.5. Receiver functions were computed using the SeisPy package (Xu & He, 2023). Following visual inspection of the radial receiver functions, three stations (BA01, BA04, and BN04) were excluded because the Moho Ps conversion was not clearly identifiable in their stacked receiver functions. Consequently, data from 24 stations,

with 24–163 receiver functions per station, were retained for further analysis. A moveout correction to a reference ray parameter of 0.065 s/km was applied to the receiver functions using the corresponding layered velocity model for each station (Sadler et al., 2026). The uncertainties associated with the stacked receiver functions were quantified using bootstrap resampling with 200 iterations. The quality-control procedure is brief in supporting materials (Text S2).

3.4 Joint Inversion of receiver functions and gravity anomaly: Joint inversion of receiver functions and gravity anomalies have been widely applied to investigate crustal structure, including crustal thickness, V_p/V_s ratios, and density variations across diverse tectonic settings (Guo et al., 2019; Guy et al., 2024; Hao et al., 2023; Shi et al., 2018; Yu et al., 2015). In this study, we employ a Bayesian joint inversion framework combining receiver-function and gravity data to investigate Moho geometry and constrain the crust–mantle density contrast beneath Bangladesh. Our methodology is based on the graph-regularized, gravity-constrained receiver-function inversion framework developed and evaluated for the Los Angeles Basin by Villa et al. (2026). The inversion parameters comprise the crust–mantle density contrast, $\Delta\rho_i = \rho_{crust} - \rho_{mantle}$, and the V_p/V_s ratio of the crystalline crust at each seismic station. Following Villa and Clayton (2026), $\Delta\rho_i$ is treated as an apparent density contrast. Density contrast is independently estimated at each station, allowing it to vary spatially across the seismic array. However, estimates from neighbouring stations are linked through a spatial smoothness prior, as described below. At each station, potential Moho *Ps* conversion phases were identified by searching for positive amplitude peaks in the stacked receiver functions within a ±1.5 s time window around the predicted Ps arrival time obtained from the corresponding station-specific velocity model (Sadler et al., 2026). To ensure the reliability of the selected phases, only peaks with amplitudes exceeding twice the bootstrap standard error of the stacked receiver function were considered, with a maximum of four candidates retained per station. Each candidate was assigned a weight based on its relative amplitude and temporal proximity to the predicted arrival time: $w = \ln(A/A_{max}) - \frac{1}{2}\,[(t - t_{pred})/\,(1\ \mathrm{s})]^{2}$, where A and A_{max} represent the amplitude of an individual candidate and the maximum amplitude among the retained candidates, respectively; t is the candidate arrival time, and t_{pred} is the predicted Moho *Ps* arrival time. The candidate yielding the highest weight was selected as the representative Moho conversion time t_{Ps}. This arrival time was subsequently converted into Moho depth using the station-specific layered velocity model following the formulation of Zhu and Kanamori (2000).

$$H_i = Z_{sed,i} + \frac{t_{Ps,i} - t_{sed,i}}{\sqrt{\frac{1}{V_{s,i}^2} - p^2} - \sqrt{\frac{1}{V_{p,i}^2} - p^2}} \quad (1)$$

Using $V_{s,i} = V_{p,i}/\kappa_i$, this becomes:

$$H_i = Z_{sed,i} + \frac{t_{Ps,i} - t_{sed,i}}{\sqrt{\frac{\kappa_i^2}{V_{p,i}^2} - p^2} - \sqrt{\frac{1}{V_{p,i}^2} - p^2}} \quad (2)$$

Here, $Z_{sed,i}$ represents the sedimentary basin thickness, while $t_{sed,i}$ denotes the *Ps* delay accumulated during propagation through the sedimentary layers. Both parameters were calculated using the sedimentary-layer structure reported by Sadler et al. (2026). The parameter V_p represents the *P*-wave velocity of the crystalline crust from the same velocity model, and p = 0.065 *s/km* is the reference ray parameter used for stacking the receiver functions. Since the κ_i is treated as a free parameter, it is estimated jointly with the crust–mantle density contrast. The Moho *Ps* arrival time is fixed to the selected candidate, allowing the gravity observations to constrain $\Delta\rho_i$ and κ_i. The gravitational contribution of the Moho beneath each station is approximated using a Bouguer slab formulation, analogous to the approach adopted by Villa et al. (2026) for estimating the gravity contribution of the sedimentary layer. A free gravity offset, g_0 is also introduced to account for the background gravity level:

$$g_i^{pred} = g_0 + 2\pi G \Delta\rho_i H_i \quad (3)$$

Here, G denotes the universal gravitational constant. The offset parameter, g_0 accounts for the regional background level of the GMRA, including contributions from sources other than Moho topography. As an alternative forward-modelling approach, we also employ the Parker (1973) Fourier-domain expansion, generalized to accommodate lateral variations in the crust–mantle density contrast.

$$F\{\Delta g\}(k) = 2\pi G e^{-|k|z_0} \sum_{n=1}^{N} \frac{(-|k|)^{n-1}}{n!} \times F\{\Delta\rho(x) h^n(x)\} \quad (4)$$

where

$$h(x) = H(x) - z_0$$

Here $\mathcal{F}$ denotes the two-dimensional Fourier transform, $\boldsymbol{k}$ the horizontal wavenumber vector and $\boldsymbol{x}$ the horizontal position. $H(\boldsymbol{x})$ is the Moho-depth field and $\Delta\rho(\boldsymbol{x})$ the density-contrast field ($\rho_{crust} - \rho_{mantle}$), with Moho relief h measured positive downward from a reference depth z_0. The gravity misfit is assumed Gaussian with a standard deviation of = 3 mGal. Within the bounds, the logarithm of the posterior probability density is therefore:

$$log\ log\ P = -\frac{1}{2}\sum_i \left(\frac{g_i^{obs} - g_i^{pred}}{\sigma_g}\right)^2 - \frac{1}{2}\sum_i \left(\frac{\Delta\rho_i - \mu_i}{\sigma_\rho}\right)^2 - \frac{\lambda_\rho}{2\sigma_\rho^2}\Delta\rho^T L \Delta\rho$$
$$-\frac{1}{2}\sum_i \left(\frac{\kappa_i - \kappa_i^0}{\sigma_\kappa}\right)^2 - \frac{\lambda_\kappa}{2\sigma_\kappa^2}\kappa^T L \kappa$$
$$+ const. \qquad (5)$$

outside the bounds the probability is zero.

The posterior distributions were explored using the Markov chain Monte Carlo (MCMC) ensemble sampler of Foreman-Mackey et al. (2013), employing 100 walkers. The sampling scheme combined differential-evolution moves (80%; ter Braak, 2006) and snooker moves (20%; ter Braak & Vrugt, 2008). Bayesian sampling has been widely applied to receiver-function inversion problems (Bodin et al., 2012). Following an initial burn-in period of 3,000 steps, the chains were advanced for 25,000 steps for the main model and 13,000 steps for the Parker model and alternative-prior configurations. To reduce sample redundancy, every tenth sample was retained for subsequent analysis. Chain convergence was evaluated using the integrated autocorrelation time, which ranged from 302 to 510 steps across the parameters. Accordingly, the production chains were approximately 30–49 times longer than the maximum autocorrelation times, yielding at least 2,900 effectively independent samples per parameter. A convergence test involving an extension of the main-model chains from 13,000 to 25,000 steps resulted in changes of less than 0.3 kg/m³ in the estimated density contrasts and less than 0.3 km in the Moho depths. The posterior median (50th percentile) was adopted as the representative estimate for each parameter, while the 16th and 84th percentiles were used to quantify the associated uncertainty. The preparation of the gravity mantle residual anomaly (GMRA), selection of the reference depth, and specification of the prior model parameters are described in detail in the Supporting Information (Text S3).

3.5 Depth-Dependent, Magma-Assisted Rifting: An analytical model incorporating non-uniform (or depth-dependent) lithospheric stretching and magmatic additions is employed to

predict post-rift sediment thickness as a function of present-day crustal thickness (Lang et al., 2026). The model integrates three main components: i) instantaneous two-layer (depth-dependent) lithospheric stretching, allowing the mantle lithosphere to undergo greater thinning than the crust; ii) magmatic additions to the crust, including underplating and seaward-dipping reflectors , which influence the stretching factors estimated from crustal thickness; and iii) an isostatic conversion of water-loaded subsidence into sediment thickness, accounting for changes in sediment density associated with compaction (Text S4). Three free parameters are statistically estimated by fitting the model predictions to gridded crustal and sediment thickness data from Bangladesh: the initial crustal thickness at the onset of magmatic addition (MA_0), the rate of magmatic addition ($\Delta MA/\Delta CT$), and the ratio of mantle-lithosphere stretching to crustal stretching (β_{ratio}). The mathematical formulation and detailed description of the model parameters are provided in the Supporting Information (Text S4).

4. Results

4.1 Gravity signal over Bangladesh: The sediment thickness exceeds 8 km, reaching a maximum of 20 km in the onshore Bengal Basin and 10–14 km in the Surma Basin (Fig. 2b). Despite the considerable sediment thickness, the Bouguer gravity anomaly over the onshore Bengal Basin varies from −8 to −32 mGal, whereas it reaches approximately −80 mGal in the Surma Basin (Fig. 3a). The GMRA over the onshore Bengal Basin ranges from 150 to 280 mGal, compared to 150–180 mGal in the Surma Basin (Fig. 3b). A strong and prominent positive anomaly is observed at the crust–mantle interface beneath Bangladesh relative to the adjacent regions. However, this significant contrast is not apparent in the Bouguer gravity anomaly, as the Indian Craton also exhibits a similar magnitude of Bouguer anomaly (Fig. 3)

4.2 Variation in Moho Topography and Crust-Mantle Density contrast: The radial components of the receiver functions were stacked for all stations, revealing two sedimentary signals at approximately 1 and 4 s, followed by a Moho *Ps* conversion at 5.6–7.4 s after the direct *P* wave (Fig. 4a). Joint inversion using the ECM1 prior model (Mooney et al., 2023) yielded Moho depths ranging from 27.2 to 38.5 km, with a mean of 31.2 km, in the Bouguer slab model (Fig. 4c & 5a). In addition to the slab model, Parker's method was also used for gravity calculations (hereafter referred to as the Parker model), yielding Moho depths ranging from 26.9 to 35.8 km, with a mean of 31.2 km, at 16 stations (Fig. S2). The posterior uncertainties in Moho depth, calculated as half the 16th–84th percentile range, are 1.8–6.7 km (median: 2.6 km) for the Bouguer slab model and 2.0–6.6 km (median: 2.4 km) for the Parker model. The crystalline

crust is 13.5–25.3 km thick (median: 16.5 km) in the Bouguer slab model and 13.8–19.3 km thick (median: 17.0 km) in the Parker model. The crustal V_p/V_s ratio ranges from 1.82 to 1.94 in the Bouguer slab model and from 1.75 to 1.91 in the Parker model (Fig. S3). At the retained stations, the Moho depths estimated using Parker's method differ from those obtained using the Bouguer slab model by −0.5 to +3.0 km, with a mean difference of +0.5 km. Three different prior models (i: global basin, ii: V_p from Sadler et al., 2026, and iii: composite-model, Fig. S4) were tested to evaluate the sensitivity of the method to the choice of prior model (Figs. S5 – S10). All three prior models yield Moho depths that differ insignificantly from those obtained using the ECM1 prior, with maximum differences of 0.5 km (median: 0.1 km) in the Bouguer slab model and 0.4 km (median: 0.1 km) in the Parker model (Figs. S5 – S10).

With the ECM1 prior, the crust–mantle density contrast ranges from −429 to −295 kg/m³ (mean: −379 kg/m³) in the Bouguer slab model (Figs. 4b, 5b, 6). In the Parker model, it ranges from −448 to −370 kg/m³ (mean: −407 kg/m³). The posterior uncertainties, calculated as half the 16th–84th percentile range, are ±21–27 kg/m³ and ±48–67 kg/m³, respectively. At the retained stations, the Parker model yields a density contrast that is, on average, 29 kg/m³ more negative than that of the Bouguer slab model (range: −81 to +36 kg/m³; r = 0.35). Assuming an upper-mantle density of 3342 kg/m³ (ECM1; Mooney et al., 2023), the bulk crustal density ranges from 2913 to 3047 kg/m³ (mean: 2963 kg/m³) in the Bouguer slab model and from 2894 to 2972 kg/m³ (mean: 2935 kg/m³) in the Parker model (Fig. 6). The predicted gravity fits the GMRA anomaly with RMS residuals of 0.16 mGal (Bouguer slab model, 24 stations) and 1.63 mGal (Parker model, 16 retained stations; 2.72 mGal for all 24 stations) (Fig. S11). The close fit obtained with the slab model is expected by construction, as each station has its own density contrast. Considering all four prior models, the density contrast ranges from −443 to −276 kg/m³ (mean: −377 kg/m³) in the Bouguer slab model and from −480 to −339 kg/m³ (mean: −403 kg/m³) in the Parker model. The corresponding mean bulk crustal densities are 2965 and 2939 kg/m³, respectively (Fig. 6). The station-wise density contrasts obtained using the four prior models show correlations of $r \geq 0.998$ in the Bouguer slab model and $r \geq 0.63$ in the Parker model. Relative to the ECM1 prior, the density contrast is, on average, 13 kg/m³ more negative with the constant prior, 22 kg/m³ less negative with the global basin prior, and 0.2 kg/m³ more negative with the Sadler *Vp* prior in the Bouguer slab model. In the Parker model, the corresponding differences are −12, +18, and +8 kg/m³, respectively (prior minus ECM1). At individual stations, the density contrasts obtained using the other prior models differ from

those obtained using the ECM1 prior by a maximum of 24 kg/m³ in the Bouguer slab model and 36 kg/m³ in the Parker model.

5. Discussion

5.1 Nature of the crust beneath the Bengal Basin: Seismological investigations, based on receiver functions and joint inversion of seismic observables, generally suggest a relatively thin crystalline crust beneath the deep basin, commonly interpreted as extended continental crust that may have undergone substantial mafic modification during Cretaceous rifting (Singh et al., 2016; Mitra et al., 2018; Wang et al., 2019; Sadler et al., 2026). In contrast, gravity-based interpretations favour the presence of oceanic or transitional crust beneath much of Bangladesh, with the Barisal–Chandpur gravity high commonly considered a possible marker of the boundary between extended continental crust to the west and oceanic crust to the east (Rajasekhar & Mishra, 2008; Krishna et al., 2022). More recent investigations have further highlighted the complexity of the crustal architecture, including substantial variations in basin depth and crystalline crustal thickness across the region (Carchedi et al., 2025; Sadler et al., 2026). In this context, we integrated gravity and receiver-function analysis provides new constraints on the Moho geometry, crystalline crustal thickness and bulk density beneath the Bengal Basin.

The density contrast between the crystalline crust and the underlying mantle provides an additional constraint on the nature of the crust beneath the basin. Our inversion yields a mean crust–mantle density contrast of −377 kg m^{-3} from Bouguer slab model, and −403 kg m^{-3} from Parker model (Fig. 6a & 6b). This range encompasses the ECM1 value of −386 kg m^{-3} reported for the region (Mooney et al., 2023). Assuming an ECM1 uppermost-mantle density of 3342 kg m^{-3} (Vp_n = 8.141 km s^{-1}), the inferred bulk density of the crystalline crust is 2965 ± 33 kg m^{-3} in the Bouguer slab model, with station-wise values ranging from 2900 to 3070 kg m^{-3}. In the Parker model it is 2939 ± 30 kg m^{-3}, with station values from 2860 to 3000 kg m^{-3} (Figures 6c and 6d). These results suggest that the bulk density of the crystalline crust beneath the basin lies broadly between 2939 and 2965 kg m^{-3}, depending on the assumed mantle reference density and gravity model. With the ECM1 uppermost-mantle density, the inferred crystalline-crust density is approximately 59–85 kg m^{-3} higher than the global mean bulk density of continental crust (2880 ± 50 kg m^{-3}; Stephenson et al., 2024). The relatively high bulk density suggests that the crust contains a substantial proportion of dense, potentially mafic, material. A comparable crustal configuration was proposed by Krishna et al. (2022), who modelled a

crust with a density of 2900 kg m^{-3} overlying a denser, approximately 3000 kg m^{-3} underplated layer. Their model suggests an underplate thickness of 2–6 km beneath the Bengal Basin, increasing to as much as 8 km beneath the Surma Basin.

The density contrast between the crystalline crust and the underlying mantle provides an additional constraint on the nature of the crust beneath the basin. Our inversion yields a mean crust–mantle density contrast of −377 kg m^{-3} from Bouguer slab model, and −404 kg m^{-3} from Parker model (Fig. 6a & 6b). This range encompasses the ECM1 value of −386 kg m^{-3} reported for the region (Mooney et al., 2023). Assuming an ECM1 uppermost-mantle density of 3342 kg m^{-3} (Vp_n = 8.141 km s^{-1}), the inferred bulk density of the crystalline crust is 2960 ± 30 kg m^{-3} in the Bouguer slab model, with station-wise values ranging from 2910 to 3050 kg m^{-3}. The Parker model yields a mean bulk crustal density of 2940 kg m^{-3} (Fig. 6). These results suggest that the bulk density of the crystalline crust beneath the basin lies broadly between 2910 and 3050 kg m^{-3}, depending on the assumed mantle reference density and gravity model. With the ECM1 uppermost-mantle density, the inferred crystalline-crust density is approximately 55–83 kg m^{-3} higher than the global mean bulk density of continental crust (2880 ± 50 kg m^{-3}; Stephenson et al., 2024). The relatively high bulk density suggests that the crust contains a substantial proportion of dense, potentially mafic, material. A comparable crustal configuration was proposed by Krishna et al. (2022), who modelled a crust with a density of 2900 kg m^{-3} overlying a denser, approximately 3000 kg m^{-3} underplated layer. Their model suggests an underplate thickness of 2–6 km beneath the Bengal Basin, increasing to as much as 8 km beneath the Surma Basin.

Independent seismic observations provide further support for the presence of relatively dense material within the lower crust beneath the Bengal Basin. Receiver-function studies have reported lower-crustal *S*-wave velocities exceeding 4.0 km s^{-1} beneath sedimentary sequences 15–17 km thick in Bangladesh (Singh et al., 2016). Beneath the northern part of the basin, approximately 9 km of lower crust with an *S*-wave velocity of 4.2 km s^{-1} overlies a Moho at approximately 44 km depth (Mitra et al., 2005). A similar high-velocity feature has been identified east of the Hinge Zone at Agartala, where the lower crust contains a roughly 6-km-thick high-velocity layer. Notably, this feature is absent beneath Kharagpur, west of the Hinge Zone, on the continental side (Mitra et al., 2008). Deep seismic sounding results also reveal anomalously high velocities beneath the Bengal Basin. Rajasekhar and Mishra (2008) identified a layer with a P-wave velocity of 7.5 km s^{-1}, which they interpreted as magmatically underplated material with a density of approximately 3100 kg m^{-3}. Similarly, Mall et al. (1999)

associated deep-seated seismic features beneath the basin with possible plume-related magmatic activity. Seismic studies conducted across the onshore and offshore Bengal Basin indicate that crustal P-wave velocities range from 6.4 to 7.4 km s^{-1}, with corresponding densities of 2700–3080 kg m^{-3} (Sadler et al., 2026; Sibuet et al., 2016). Based on a crystalline-crustal *P*-wave velocity of 6.7 km s^{-1}, Sadler et al. (2026) suggested that the crust beneath the basin is faster than typical continental crust but slower than typical oceanic crust. Collectively, these observations point towards a heterogeneous crystalline crust containing relatively high-velocity and high-density lower-crustal material. The relatively thin crystalline crust has been also attributed to continental stretching accompanied by mafic intrusions and possible magmatic underplating associated with the Early Cretaceous Kerguelen plume activity (Storey et al., 1992; Sadler et al., 2026; Singh et al., 2016). However, alternative interpretations invoke oceanic crust formation or subduction-related crustal structures beneath the eastern Bengal Basin (Krishna et al., 2022; Rajasekhar & Mishra, 2008; Wang et al., 2019; Carchedi et al., 2025).

A high bulk density does not resolve the ambiguity, because it is expected both for heavily intruded continental crust and for thickened igneous oceanic crust. Therefore, we further investigate whether the relatively thin, dense crust is better interpreted as strongly attenuated continental crust modified by magmatism or as transitional to thickened oceanic crust. The crustal V_p/V_s ratios obtained from our Bouguer slab model range from 1.82 to 1.94 (Fig. S3). These values are largely inherited from the velocity models of Sadler et al. (2026) and are notably higher than the value of 1.73 ± 0.01 reported beneath Kharagpur, west of the Hinge Zone (Mitra et al., 2008). Elevated V_p/V_s ratios have also been associated with magmatic modification of the lower crust in other extensional settings. For example, a joint receiver-function and gravity investigation of extensional basins in northeastern China attributed high V_p/V_s ratios above a shallow Moho to the intrusion of hot, mantle-derived material (Hao et al., 2023). Although elevated V_p/V_s ratios alone do not uniquely establish a magmatic origin, their occurrence together with relatively high seismic velocities and bulk densities is consistent with substantial mafic addition to the lower crust beneath the Bengal Basin. The thickness and density of the inferred dense component are also broadly comparable with those of the high-velocity lower-crustal layer reported beneath Agartala (Mitra et al., 2008) and the underplated layer proposed by Rajasekhar and Mishra (2008). These similarities suggest that a relatively thin, dense lower-crustal component could account for a substantial proportion of the elevated bulk density inferred from gravity modelling.

A plausible source of this dense lower-crustal material is magmatism associated with the Early Cretaceous breakup of eastern Gondwana and the influence of the Kerguelen plume. The Rajmahal–Sylhet flood basalts were emplaced rapidly at approximately 118 ± 2 Ma over an area exceeding 2×10^5 km², and Rajmahal-type basalts have been recovered from numerous boreholes across the Bengal Basin (Ray et al., 2005). Seaward-dipping reflectors, interpreted as volcanic sequences, have also been identified along a seismic profile crossing the Hinge Zone south of the Shillong Plateau (Talwani et al., 2016). Furthermore, gravity models along the eastern margin of the Indian Shield are consistent with a volcanic rifted margin characterised by seaward-dipping reflectors and magmatically underplated material (Krishna et al., 2022). These geological and geophysical observations provide a plausible tectono-magmatic context for the incorporation of dense mafic material into the lower crust during Cretaceous rifting. Although our gravity and receiver-function results do not uniquely establish the origin of this material, they are consistent with substantial magmatic modification of the crust during the breakup of eastern Gondwana. Notably, the inferred density and seismic velocity of the crystalline crust are comparable to those of normal oceanic crust and large igneous province-related oceanic crust in the ECM1 compilation. The plume-related magmatic activity has thickened the oceanic crust beneath the Greenland–Iceland–Faroe Ridge to approximately 25–30 km (Thybo & Artemieva, 2013). Thus, our results establish the presence of a relatively thin, dense crystalline crust beneath the Bengal Basin, consistent with substantial mafic modification associated with Early Cretaceous rifting and magmatism.

5.2 Anomalous subsidence beneath the Bangladesh Margin: One of the distinctive features of Bangladesh is the presence of an exceptionally deep sedimentary basin, with sediment thickness reaching 15–20 km, together with magmatic additions associated with the Kerguelen plume at approximately 120–118 Ma (Fig. 7). Basement subsidence in the Bangladesh commenced during the Early Cretaceous (~120 Ma), following the breakup of microcontinental fragments along the Rajmahal–Sylhet Traps line, and has continued alongside sediment accumulation throughout much of the basin's evolution, with enhanced sediment influx generally accompanying increased subsidence rates (Alam et al., 2003; Frielingsdorf et al., 2008; Talwani et al., 2016). This subsidence remains active in the delta plain during the Holocene, with rates increasing towards the coast, from less than 0.2 mm/yr inland of the Hinge Zone to 4 ± 1.4 mm/yr in the lower tidal delta (Grall et al., 2018). To investigate the formation of 15-20 km deep sedimentary basin along a volcanic rifted margin, particularly the roles of lithospheric extension and magmatic addition to the crust (Lu & Huismans, 2021), we apply

the non-uniform, magma-assisted rifting model of Lang et al. (2026) to the observed crustal and sediment thicknesses across the extended continental domain of Bangladesh (Fig. 7). The bootstrap analysis of the three free parameters (MA_0, $\Delta MA/\Delta CT$ and β_{ratio}) provides insights into the nature of lithospheric deformation and magmatic modification during rifting. The results indicate that mantle lithospheric thinning is approximately 2 – 3 times greater than crustal thinning, while magmatic addition increases at a rate of 1.25 km for every kilometre of crustal thinning ($\Delta MA/\Delta CT$ = 1.25 km/km), with magmatic addition initiating at an initial thickness of MA_0 = 28.0 km (Fig. 7d). The lithosphere thickness reduces from 125 km to 90 km beneath the Bangladesh (Saha et al., 2021). Although the non-uniform, magma-assisted rifting model reproduces the general relationship between sediment thickness and present-day crustal thickness, it fails to account for observations where sediment thickness exceeds 12.5 km (Fig. 7c). The inability of the non-uniform, magma-assisted rifting model to reproduce the exceptionally thick sedimentary succession suggests that additional geodynamic and sedimentary processes may have contributed to subsidence and accommodation generation in the Bengal Basin. Mantle convection can produce long-wavelength negative dynamic topography (0.6 – 1.0 km in west Bangladesh, Stephenson et al., 2024; Zheng et al., 2026), resulting in additional subsidence beyond that predicted by lithospheric stretching and thermal relaxation (Davies et al., 2019; Heine et al., 2008). Furthermore, ductile deformation and lateral redistribution of lower-crustal material may influence crustal architecture and long-term basin evolution, particularly in regions affected by substantial tectonic loading (Beaumont et al., 2001). Progressive sediment accumulation also increases the load on the underlying lithosphere, while burial-related compaction reduces sediment porosity and modifies the sedimentary thickness and subsidence history (Sclater & Christie, 1980; Steckler et al., 2024). The anomalous subsidence (1.1 – 7 mm/yr) in the Bengal Basin varies spatially and temporally, reflecting the combined effects of long-term lithospheric adjustment, sediment loading, and shallow sediment compaction (Karpytchev et al., 2018; Steckler et al., 2024). Although these processes represent plausible additional contributions, their relative importance in the Bengal Basin remains to be quantified. Integrating these mechanisms into a coupled lithospheric and basin-evolution model may therefore provide a more comprehensive explanation for the observed sediment thicknesses and the associated anomalous subsidence. Figure 8 presents a schematic illustration of the tectonic evolution and development of the sedimentary basin in Bangladesh.

6. Conclusions:

This study presents an integrated geophysical approach for estimating bulk crystalline crustal density through the joint inversion of teleseismic receiver functions and gravity anomaly data. Unlike conventional approaches that estimate density from seismic velocity using empirical velocity–density relationships, our method exploits the complementary sensitivities of the two datasets. The joint inversion of receiver-function and gravity data reveals substantial lateral variations in crustal thickness of 13.5 – 25.3 km and bulk crustal density of 2910 – 3050 kg m^{-3}, together with elevated V_p/V_s ratios (1.82–1.94), suggests substantial mafic modification of the crust, potentially associated with magmatic intrusion and underplating associated with Kerguelen plume. The important distinction is that you are not simply converting seismic velocity into density using an empirical relationship. Instead, gravity provides an independent constraint on the crustal density structure, while receiver functions help constrains the geometry of the crust–mantle boundary. The non-uniform, magma-assisted rifting model indicates preferential thinning of the mantle lithosphere relative to the crust, with a β_{ratio} of 2 - 3 and magmatic addition increasing by 1.25 km per kilometre of crustal thinning. These results support a significant role for magmatism in modifying the lithosphere during basin development. The rifting model fails to reproduce sediment thicknesses exceeding 12.5 km, indicating that lithospheric stretching and magmatic addition alone cannot explain the exceptionally deep Bengal Basin. Additional contributions from mantle-driven dynamic topography, lower-crustal deformation, sediment loading and compaction are plausible mechanisms for generating the observed anomalous subsidence. Overall, the results suggest that the evolution of the Bengal Basin reflects the combined influence of Early Cretaceous extension, magmatic modification and subsequent long-wavelength subsidence. Further integration of geophysical constraints with coupled lithospheric and basin-evolution models is required to resolve the relative contributions of these processes.

Acknowledgements:

MI and MR acknowledge the generous funding support from Anusandhan National Research Foundation (ANRF) sponsored PM-ECRG grant (sanction order number: ANRF/ECRG/2024/000776/EAS). All figures were prepared using GMT (Generic Mapping Tools; Wessel et al., 2019) and Python-based visualization libraries.

Data Availability:

The SRTM15+ topography data is downloaded from Tozer et al. (2019) (https://www.ngdc.noaa.gov/mgg/global/). The BIMA (Tripartite-BIMA (Bangladesh-India-

Myanmar Array) and XI passive seismic waveform data are publicly available through the FDSN network (Sandvol et al., 2018; Seeber et al., 2007) and can be accessed at https://www.fdsn.org/networks/detail/XR_2018/, https://www.fdsn.org/networks/detail/XI_2007/ . The satellite-derived bathymetry and free-air gravity anomaly data in the ocean domain are publicly accessible at https://topex.ucsd.edu. The land-acquired Bouguer gravity anomaly data for Bangladesh are available in public domain by USGS (doi:10.3133/ofr97470H).

Code Availability

The Seispy package is available in public domain (https://github.com/xumi1993/seispy) and Graph-Regularized Bayesian Approach for Gravity-Informed Mapping (GravNet) software is publicly available at Villa (2025) https://doi.org/10.5281/zenodo.17728056. The revised code for crustal structure will be made available on request. The python code for non-uniform magma-addition driven basin subsidence is available on https://zenodo.org/records/20395298.

Conflict of Interest

The authors declare no competing interests.

Author Contributions

M. Rishal: Formal analysis, methodology, software, validation, visualization, and writing – original draft. M. Ismaiel: Conceptualization, methodology, investigation, supervision, interpretation, visualization, and writing – original draft, review and editing.

References:

Acharyya, S.K. (2007). Collisional emplacement history of the Naga-Andaman ophiolites and the position of the eastern Indian suture. *J. Asian Earth Sci.*, *29*, 229–242.

Alam, M., Alam, M.M., Curray, J. R., Chowdhury, M.L.R., & Gani, M.R. (2003). An overview of the sedimentary geology of the Bengal Basin in relation to the regional tectonic framework and basin-fill history. *Sedimentary Geology*, *155*(3–4), 179–208.

Arora, B. R., Prajapati, S.K., Saikia, S., & Bansal, B.K. (2024). Crustal structure of Northeast India as evidenced by receiver function imaging: tectonic and geodynamic implications. *International Journal of Earth Sciences*, *113*(3), 733-755.

Thybo, H., & Artemieva, I. M. (2013). Moho and magmatic underplating in continental lithosphere. Tectonophysics, 609, 605–619.

Asimus, J. L., Halpin, J. A., Daczko, N. R., Whittaker, J. M., Coffin, M. F., Belousov, I., et al. (2025). Discovery of the William's Ridge and Rig Seismic Seamount microcontinents, Kerguelen Plateau: Signatures of a fragmented rifted margin. *Tectonics*, 44, e2025TC008958.

Beaumont, C., Jamieson, R. A., Nguyen, M. H., & Lee, B. (2001). Himalayan tectonics explained by extrusion of a low-viscosity crustal channel coupled to focused surface denudation. Nature, 414, 738–742.

Betka, P.M., Seeber, L., Thomson, S.N., Steckler, M.S., Sincavage, R., & Zoramthara, C. (2018). Slip-partitioning above a shallow, weak décollement beneath the Indo-Burman accretionary prism. *Earth and Planetary Science Letters*, *503*, 17-28.

Bodin, T., Sambridge, M., Tkalčić, H., Arroucau, P., Gallagher, K., & Rawlinson, N. (2012). Transdimensional inversion of receiver functions and surface wave dispersion. Journal of geophysical research: solid earth, 117(B2).

Bürgi, P., Hubbard, J., Akhter, S.H., Peterson, D.E., 2021. Geometry of the d´ecollement below eastern Bangladesh and implications for seismic hazard. *J. Geophys. Res. Solid Earth*, *126*, e2020JB021519.

Carchedi, C.J., Gaherty, J.B., Byrnes, J.S., Rondenay, S., Steckler, M.S., Ajala, R., ... & Akhter, S.H. (2025). Evolving sediment structure and lithospheric architecture across the Indo-Burman forearc margin from the joint inversion of surface-and scattered-wave seismic constraints. *Journal of Geophysical Research: Solid Earth*, *130*(6), e2024JB030050.

Curray, J.R., & Moore, D.G. (1971). Growth of the Bengal deep-sea fan and denudation in the Himalayas. *Geological Society of America Bulletin*, *82*(3), 563-572.

Curray, J.R. (1991). Possible greenschist metamorphism at the base of a 22-km sedimentary section, Bay of Bengal. *Geology*, *19*(11), 1097-1100.

Damodara, N., Rao, V.V., Sain, K., Prasad, A.S.S.S.R.S., & Murty, A.S.N. (2017). Basement configuration of the West Bengal sedimentary basin, India as revealed by seismic refraction tomography: its tectonic implications. *Geophysical Journal International*, *208*(3), 1490-1507.

Davies, D. R., et al. (2019). Earth's multi-scale topographic response to global mantle flow. Nature Geoscience, 12, 845–850.

Foreman-Mackey, D., Hogg, D. W., Lang, D., & Goodman, J. (2013). emcee: the MCMC hammer. Publications of the Astronomical Society of the Pacific, 125(925), 306-312.

Frielingsdorf, J., Islam, S.A., Block, M., Rahman, M.M., Rabbani, M.G., 2008. Tectonic subsidence modeling and Gondwana source rock hydrocarbon potential, Northwest Bangladesh modeling of Kuchma, Singra and Hazipur wells. *Marine and Petroleum Geology*, *25*, 553–564.

Govin, G., Najman, Y., Copley, A., Millar, I., Van der Beek, P., Huyghe, P., ... & Davenport, J. (2018). Timing and mechanism of the rise of the Shillong Plateau in the Himalayan foreland. *Geology*, *46*(3), 279-282.

Grall, C., Steckler, M. S., Pickering, J. L., Goodbred, S., Sincavage, R., Paola, C., ... & Spiess, V. (2018). A base-level stratigraphic approach to determining Holocene subsidence of the Ganges–Meghna–Brahmaputra Delta plain. *Earth and Planetary Science Letters*, *499*, 23-36.

Guo, L., Gao, R., Shi, L., Huang, Z., & Ma, Y. (2019). Crustal thickness and Poisson's ratios of South China revealed from joint inversion of receiver function and gravity data. Earth and Planetary Science Letters, 510, 142-152.

Guy, A., Tiberi, C., & Mijiddorj, S. (2024). Crustal structures from receiver functions and gravity modeling in central Mongolia. Journal of Geophysical Research: Solid Earth, 129(1), e2023JB027614.

Hao, A., Zhang, H., Han, S., & Xu, W. (2023). High-resolution Moho depth and V p/V s ratio distributions in northeast China from joint inversion of receiver functions and gravity data and their geological implications. Science China Earth Sciences, 66(7), 1569-1582.

Heine, C., Müller, R. D., Steinberger, B., & Torsvik, T. H. (2008). Subsidence in intracontinental basins due to dynamic topography. Physics of the Earth and Planetary Interiors, 171, 252–264.

Hossain, M. S., Xiao, W., Khan, M. S. H., Chowdhury, K. R., & Ao, S. (2020). Geodynamic model and tectono-structural framework of the Bengal Basin and its surroundings. *Journal of Maps*, *16*(2), 445-458.

Ismaiel, M., Krishna, K.S., Srinivas, K., Mishra, J., & Saha, D. (2019). Crustal architecture and Moho topography beneath the eastern Indian and Bangladesh margins–new insights on rift evolution and the continent–ocean boundary. *Journal of the Geological Society*, *176*(3), 553-573.

Karpytchev, M., Ballu, V., Krien, Y., et al. (2018). Contributions of a Strengthened Early Holocene Monsoon and Sediment Loading to Present-Day Subsidence of the Ganges-Brahmaputra Delta. Geophysical Research Letters.

Kent, R. W., Pringle, M. S., Müller, R. D., Saunders, A. D., & Ghose, N. C. (2002). 40Ar/39Ar geochronology of the Rajmahal basalts, India, and their relationship to the Kerguelen Plateau. *Journal of Petrology*, 43(7), 1141-1153.

Khan, A.A., & Chouhan, R.K.S. (1996). The crustal dynamics and the tectonic trends in the Bengal Basin. *Journal of Geodynamics*, *22*(3-4), 267-286.

Khin, K., Zaw, K., & Aung, L. T. (2017). Geological and tectonic evolution of the Indo-Myanmar Ranges (IMR) in the Myanmar region.

Krishna, K.S., Abhimanyu, R., & Ismaiel, M. (2022). Evidence for paleo-continental margin and folding of relic fragment of oceanic lithosphere, northeast Indian subcontinent. *Marine Geology*, *453*, 106927.

Kumar, A., Mitra, S., & Suresh, G. (2015). Seismotectonics of the eastern Himalayan and Indo-Burman plate boundary systems. *Tectonics*, *34*(11), 2279-2295.

Lang, G., ten Brink, U. S., & Makovsky, Y. (2026). Rapid cooling of magma-rich margins exemplified by the Eastern North American Margin. Communications Earth & Environment, 7, 548. https://doi.org/10.1038/s43247-026-03742-2

Ligorría, J. P., & Ammon, C. J. (1999). Iterative deconvolution and receiver-function estimation. Bulletin of the seismological Society of America, 89(5), 1395-1400.

Lu, G., & Huismans, R.S. (2021). Melt volume at Atlantic volcanic rifted margins controlled by depth-dependent extension and mantle temperature. *Nature Communication*, *12*, 3894.

Mallick, R., Lindsey, E.O., Feng, L., Hubbard, J., Banerjee, P., & Hill, E.M. (2019). Active convergence of the India-Burma-Sunda plates revealed by a new continuous GPS network. *Journal of Geophysical Research: Solid Earth*, *124*(3), 3155-3171.

Mallick, R., Hubbard, J.A., Lindsey, E.O., Bradley, K.E., Moore, J.D., Ahsan, A., ... & Hill, E. M. (2020). Subduction initiation and the rise of the Shillong Plateau. *Earth and Planetary Science Letters*, *543*, 116351.

Mandal, P. (2022). Evidence of secular variation in Archean crust formation in the Eastern Indian Shield. *Scientific Reports*, *12*(1), 14040.

Maurin, T., & Rangin, C. (2009). Structure and kinematics of the Indo-Burmese Wedge: Recent and fast growth of the outer wedge. *Tectonics*, *28*(2), TC2010.

Milliman, J.D., & Farnsworth, K.L. (2013). River discharge to the coastal ocean: a global synthesis. *Cambridge University Press*.

Milliman, J.D., & Syvitski, J.P. (1992). Geomorphic/tectonic control of sediment discharge to the ocean: the importance of small mountainous rivers. *The journal of Geology*, *100*(5), 525-544.

Mitchell, A.H.G. (1981). Phanerozoic plate boundaries in mainland SE Asia, the Himalayas and Tibet. *Journal of the Geological Society*, *138*(2), 109-122.

Mitra, S., Bhattacharya, S., & Nath, S. (2008). Crustal structure of the Western Bengal Basin from joint analysis of teleseismic receiver functions and Rayleigh-wave dispersion. *Bulletin of the Seismological Society of America*, *98*(6), 2715–2723.

Mitra, S., Priestley, K.F., Borah, K., & Gaur, V.K. (2018). Crustal structure and evolution of the Eastern Himalayan plate boundary system, Northeast India. *Journal of Geophysical Research: Solid Earth*, *123*, 621–640.

Mitra, S., Priestley, K., Bhattacharyya, A. K., & Gaur, V. K. (2005). Crustal structure and earthquake focal depths beneath northeastern India and southern Tibet. Geophysical Journal International, 160(1), 227-248.

Mooney, W. D., Barrera-Lopez, C., Suárez, M. G., & Castelblanco, M. A. (2023). Earth crustal model 1 (ECM1): A 1 x 1 global seismic and density model. Earth-Science Reviews, 243, 104493.

Najman, Y., Bracciali, L., Parrish, R.R., Chisty, E., & Copley, A. (2016). Evolving strain partitioning in the Eastern Himalaya: The growth of the Shillong Plateau. *Earth and Planetary Science Letters*, *433*, 1-9.

Ni, J. F., Guzman-Speziale, M., Bevis, M., Holt, W. E., Wallace, T. C., & Seager, W. R. (1989). Accretionary tectonics of Burma and the three-dimensional geometry of the Burma subduction zone. *Geology*, *17*(1), 68-71.

Parker, R.L. (1972). The rapid calculation of potential anomalies. *Geophys J. R. astr. Soc.*, 31, 447–455.

Rajasekhar, R.P., & Mishra, D.C. (2008). Crustal structure of Bengal basin and Shillong plateau: extension of Eastern Ghat and Satpura mobile belts to Himalayan fronts and seismotectonics. *Gondwana Research*, *14*(3), 523-534.

Rangin, C., & Sibuet, J. C. (2017). Structure of the northern Bay of Bengal offshore Bangladesh: Evidences from new multi-channel seismic data. Marine and Petroleum Geology, 84, 64-75.

Ray, J. S., Pattanayak, S. K., & Pande, K. (2005). Rapid emplacement of the Kerguelen plume–related Sylhet Traps, eastern India: Evidence from 40Ar-39Ar geochronology. Geophysical Research Letters, 32(10).

Sadler, B., Persaud, P., Pulliam, J., Sandvol, E., Gaherty, J., Steckler, M. S., & Akhter, S. H. (2026). Nature of the crust in the superdeep Bengal Basin using teleseismic P waves. *Journal of Geophysical Research: Solid Earth*, 131, e2025JB031292.

Saha, G. K., Rai, S. S., Prakasam, K. S., & Gaur, V. K. (2021). Distinct lithospheres in the Bay of Bengal inferred from ambient noise and earthquake tomography. Tectonophysics, 809, 228855.

Sandvol, E., Gaherty, J., Steckler, M., & Persaud, P. (2018). Tripartite-BIMA (Bangladesh-India-Myanmar Array).

Sandwell, D.T., Müller, R.D., Smith, W.H., Garcia, E., & Francis, R. (2014). New global marine gravity model from CryoSat-2 and Jason-1 reveals buried tectonic structure. *Science*, *346*(6205), 65-67.

Sclater, J. G., & Christie, P. A. (1980). Continental stretching: An explanation of the post-mid-Cretaceous subsidence of the central North Sea basin. Journal of Geophysical Research: Solid Earth, 85(B7), 3711-3739.

Seeber, L Michael Steckler, & Won-Young Kim. (2007). Collision of the Burma Arc accretionary prism and foldbelt with the Ganges-Brahmaputra Delta in Bangladesh [Data set]. International Federation of Digital Seismograph Networks.

Shi, L., Guo, L., Ma, Y., Li, Y., & Wang, W. (2018). Estimating crustal thickness and Vp/Vs ratio with joint constraints of receiver function and gravity data. Geophysical Journal International, 213(2), 1334-1344.

Sibuet, J. C., Klingelhoefer, F., Huang, Y. P., Yeh, Y. C., Rangin, C., Lee, C. S., & Hsu, S. K. (2016). Thinned continental crust intruded by volcanics beneath the northern Bay of Bengal. *Marine and Petroleum Geology*, *77*, 471-486.

Singh, A., Bhushan, K., Singh, C., Steckler, M. S., Akhter, S. H., Seeber, L., ... & Biswas, R. (2016). Crustal structure and tectonics of Bangladesh: New constraints from inversion of receiver functions. *Tectonophysics*, *680*, 99-112.

Socquet, A., & Pubellier, M. (2005). Cenozoic deformation in western Yunnan (China–Myanmar border). *Journal of Asian Earth Sciences*, *24*(4), 495-515.

Steckler, M.S., Akhter, S.H., Seeber, L., Kopp, C., & Armijo, R. (2008). *Collision of the Ganges–Brahmaputra Delta with the Burma Arc: Implications for earthquake hazard. Earth and Planetary Science Letters*, *273*(3–4), 367–378.

Steckler, M.S., Mondal, D.R., Akhter, S.H., Seeber, L., Feng, L., Gale, J., & Nooner, S. (2016). *Locked and loading megathrust linked to active subsidence in the Ganges–Brahmaputra Delta. Nature Geoscience*, *9*(10), 838–842.

Steckler, M. S., Jaman, M. H., Grall, C. J., Goodbred, S. L., Wilson, C. A., & Oryan, B. (2024). Contribution of campaign GNSS toward parsing subsidence rates by time and depth in coastal Bangladesh. Frontiers in Earth Science, 12, 1354686.

Stephenson, S. N., Hoggard, M. J., Holdt, M. C., & White, N. (2024). Continental residual topography extracted from global analysis of crustal structure. Journal of Geophysical Research: Solid Earth, 129, e2023JB026735. https://doi.org/10.1029/2023JB026735

Stolk, W., Kaban, M., Beekman, F., Tesauro, M., Mooney, W. D., & Cloetingh, S. (2013). High resolution regional crustal models from irregularly distributed data: Application to Asia and adjacent areas. *Tectonophysics*, *602*, 55-68.

Storey, M., Kent, R. W., Saunders, A. D., Salters, V. J., Hergt, J., Whitechurch, H., ... & Gifford, M. (1992). Lower Cretaceous volcanic rocks on continental margins and their relationship to the Kerguelen Plateau. In Proceedings of the Ocean Drilling Program, scientific results (Vol. 120, pp. 33-53). College Station, TX: Ocean Drilling Program.

Talwani, M., Desa, M.A., Ismaiel, M., & Krishna, K.S., 2016. The Tectonic origin of the Bay of Bengal and Bangladesh. *Journal of Geophysical Research: Solid Earth*, *121*, 4836–4851.

Talwani, M., Krishna, K. S., Ismaiel, M., & Desa, M. A. (2017). Comment on a paper by Sibuet et al.(2016) entitled "Thinned continental crust intruded by volcanics beneath the northern Bay of Bengal". Marine and Petroleum Geology, 88, 1123-1125.

ter Braak, C. J. F. (2006). A Markov Chain Monte Carlo version of the genetic algorithm Differential Evolution: easy Bayesian computing for real parameter spaces. *Statistics and Computing*, 16, 239–249.

ter Braak, C. J. F., & Vrugt, J. A. (2008). Differential Evolution Markov Chain with snooker updater and fewer chains. *Statistics and Computing*, 18, 435–446. doi:10.1007/s11222-008-9104-9

Tozer, B., Sandwell, D.T., Smith, W.H., Olson, C., Beale, J. R., & Wessel, P. (2019). Global bathymetry and topography at 15 arc sec: SRTM15+. *Earth and Space Science*, *6*(10), 1847-1864.

Uddin, A., & Lundberg, N. (1998). Cenozoic history of the Himalayan-Bengal system: Sand composition in the Bengal basin, Bangladesh. *Geological Society of America Bulletin*, *110*(4), 497-511.

USGS - Bangladesh Gas Assessment Team (2001). In: Wandrey, C.J. (Ed.), U.S. Geological Survey-PetroBangla Cooperative Assessment of Undiscovered Natural Gas Resources of Bangladesh, Petroleum Systems and Related Geologic Studies in Region 8, South Asia, pp. 1–124 available online at. http://geology.cr.usgs.gov/pub/bulletins/b2208-a/.

Villa, V. (2025). Graph-Regularized bayesian approach for Gravity- informed mapping (GravNet) [Software]. Zenodo. https://doi.org/10.5281/zenodo.17728056

Villa, V., Li, Y., Clayton, R. W., & Persaud, P. (2023). Three-Dimensional Basin depth map of the Northern Los Angeles basins from gravity and seismic measurements. Journal of Geophysical Research: Solid Earth, 128(7), e2022JB025425. https://doi.org/10.1029/2022JB025425

Villa, V., & Clayton, R. W. (2026). Three-dimensional structure of the Los Angeles Basin and its underlying Moho. Journal of Geophysical Research: Solid Earth, 131, e2026JB033837. https://doi.org/10.1029/2026JB033837

Vorobieva, I., Gorshkov, A., & Mandal, P. (2021). Modelling the seismic potential of the Indo-Burman megathrust. *Scientific Reports*, *11*(1), 21200.

Wang, X., Wei, S., Wang, Y., Maung Maung, P., Hubbard, J., Banerjee, P., ... & Almeida, R. (2019). A 3-D shear wave velocity model for Myanmar region. *Journal of Geophysical Research: Solid Earth*, *124*(1), 504-526.

Welford, J.K. (2024). Magma-poor continent–ocean transition zones of the southern North Atlantic: a wide-angle seismic synthesis of a new frontier. Solid Earth, 15(6), 683-710.

Wessel, P., Luis, J.F., Uieda, L., Scharroo, R., Wobbe, F., Smith, W.H.F., & Tian, D. (2019). *The Generic Mapping Tools version 6. Geochemistry, Geophysics, Geosystems*, *20*(11), 5556–5564.

Xu, M., & He, J. (2023). Seispy: Python module for batch calculation and postprocessing of receiver functions. Seismological Society of America, 94(2A), 935-943.

Yu, Y., Liu, K. H., Reed, C. A., Moidaki, M., Mickus, K., Atekwana, E. A., & Gao, S. S. (2015). A joint receiver function and gravity study of crustal structure beneath the incipient Okavango Rift, Botswana. Geophysical Research Letters, 42(20), 8398-8405.

Zheng, T., He, Y., Ding, L., Jiang, M., Ai, Y., Mon, C. T., ... & Thant, M. (2020). Direct structural evidence of Indian continental subduction beneath Myanmar. Nature Communications, 11(1), 1944.

Zhang, Y., Müller, D., & Seton, M. (2026). Negative residual topography in global back-arc basins scales with slab dip. Geophysical Research Letters, 53, e2026GL124421. https://doi.org/10.1029/2026GL124421

Zhu, L., & Kanamori, H. (2000). Moho depth variation in southern California from teleseismic receiver functions. Journal of Geophysical Research: Solid Earth, 105(B2), 2969-2980.

Figure Captions

Figure 1: (a) Elevation map of northeastern India (SRTM15+; Tozer et al., 2019), showing major morphological features, including the Indo-Burma Ranges, Shillong Plateau, and Chotanagpur Plateau, which form elevated regions surrounding the relatively flat sedimentary basin. The inset map shows the location of the study area in the context of the regional topography of the Indian Peninsula and adjacent oceans. (b) Locations of the seismic stations used in the present study, shown as red filled circles. (c) Schematic lithospheric structure extending from the Indian Shield/craton to the Indo-Burma Ranges (IBR), illustrating the subduction of the Indian Plate beneath the Burmese lithosphere.

Figure 2: a) Geological map of the study region showing the distribution of major geological units and tectonic structures. The Rajmahal and Sylhet Traps represent volcanic sequences associated with the Kerguelen plume activity during approximately 120–115 Ma. Tertiary sedimentary successions occupy the sedimentary basins of Bangladesh. Major normal faults and subduction zones are also indicated. GKF = Garhmoyna–Khandaghosh Fault; JGF = Jangipur–Gaibandha Fault; MKF = Malda–Kishanganj Fault; PF = Pingla Fault; SBF = Sainthia–Bahmani Fault; RF = Rajmahal Fault. b) Spatial distribution of sediment thickness across northeastern India, illustrating substantial sediment accumulation within the Bengal Basin, where the thickness reaches approximately 20 km. The Sylhet Trough (Surma Basin) also exhibits considerable sediment accumulation, with thicknesses of approximately 12–14 km. Red circles denote the locations of publicly available broadband seismic stations used in this study to estimate Moho depths.

Figure 3: a) Bouguer gravity anomaly over the continental region and free-air gravity anomaly over the offshore region (adopted from Krishna et al., 2022). b) Mantle residual gravity anomaly estimated by removing the gravity contributions from sediments, thermal and pressure variations, and deeper sources.

Figure 4: (a) Stacked radial receiver functions (1,426 receiver functions in total; Gaussian factor 2.5). Yellow stars joined by the solid blue line mark the Moho Ps conversion, picked 5.6–7.4 s after the direct P wave. The light-blue and pink dashed lines follow earlier conversions from within the sedimentary basin (about 1 s) and from its base (3.5–4.3 s). The column on the right shows the corresponding layers: sediment, crystalline crust and upper mantle. (b) Observed gravity mantle residual anomaly (GMRA, mGal; yellow stars) and the anomaly predicted by the inversion (blue line). (c) Moho depth (km) from this study (green

circles) compared with Sadler et al. (2026) (red squares). (d) Crust–mantle density contrast, Δρ (kg/m³; posterior median, blue circles). The pale-yellow band shows the ECM1 prior (Mooney et al., 2023), and the dashed line marks its mean.

Figure 5: Map view of the main model (Bouguer slab, ECM1 prior) at the 24 stations: (a) Moho depth (km) and (b) crust–mantle density contrast, Δρ (kg/m³; posterior medians), shown over shaded topographic relief.

Figure 6: Sensitivity of the results to the prior density model. (a) Density contrast, Δρ (kg/m³), in the Bouguer slab model. (b) Density contrast, Δρ (kg/m³), in the Parker model. (c) Bulk crustal density, ρc (g/cm³), in the Bouguer slab model. (d) Bulk crustal density, ρc (g/cm³), in the Parker model. The average crustal density estimated using the Bouguer slab model is 2965 kg/m³, whereas the Parker model yields an average density of 2938 kg/m³.

Figure 7: a) – b) Variations in sediment thickness and crustal thickness along the eastern Bangladesh margin. Sediment thickness increases from approximately 2 km beneath the Indian Craton to 17 km beneath the onshore Bengal Basin, whereas crustal thickness exhibits an opposite trend. c) – d) Statistical fitting of sediment thickness versus crustal thickness data for the magma-rich Bangladesh margin. Histograms showing the distributions of the three free parameters are presented in the bottom panels.

Figure 8: A schematic diagram illustrating the development of the sedimentary basin beneath Bangladesh. The volcanic rifted margin formed around 120 Ma, followed by continuous sediment deposition from the Ganges–Brahmaputra river system. Subduction of the Indian Plate beneath the Burma Plate initiated approximately 50 Ma. The Bengal Basin has accumulated an exceptionally thick sedimentary sequence exceeding 15 km, suggesting that additional geodynamic processes, beyond conventional plate-cooling models, are required to explain its subsidence.

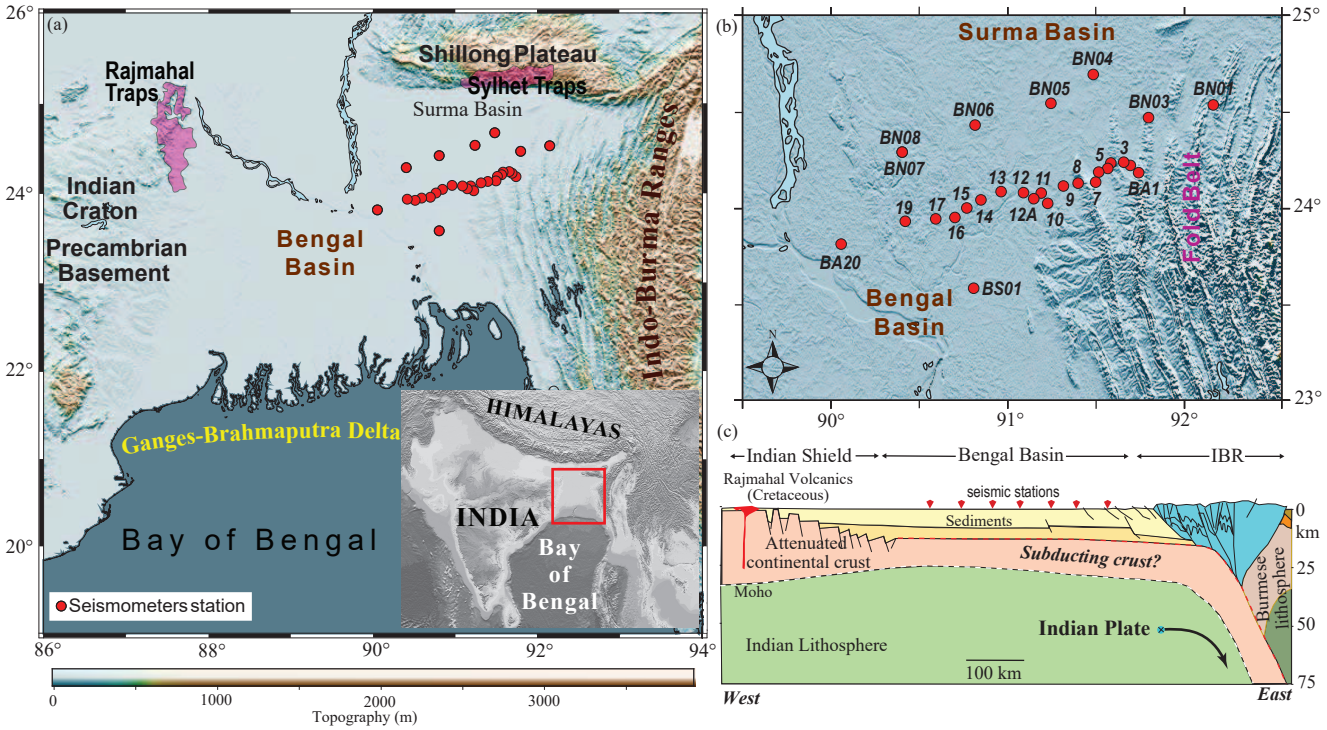

(a)
Rajmahal Traps
Shillong Plateau
Sylhet Traps
Surma Basin
Indian Craton
Precambrian Basement
Bengal Basin
Indo-Burma Ranges
Ganges-Brahmaputra Delta
HIMALAYAS
INDIA
Bay of Bengal
Bay of Bengal
Seismometers station
26°
24°
22°
20°
86°
88°
90°
92°
94°
0
1000
2000
3000
Topography (m)
(b)
Surma Basin
BN04
BN05
BN06
BN03
BN01
BN08
BN07
BA1
BA20
BS01
Bengal Basin
Fold Belt
N
25°
24°
23°
90°
91°
92°
(c)
Indian Shield
Bengal Basin
IBR
Rajmahal Volcanics (Cretaceous)
seismic stations
Sediments
Attenuated continental crust
Subducting crust?
Moho
Indian Lithosphere
Indian Plate
100 km
Burmese lithosphere
0 km
25
50
75
West
East

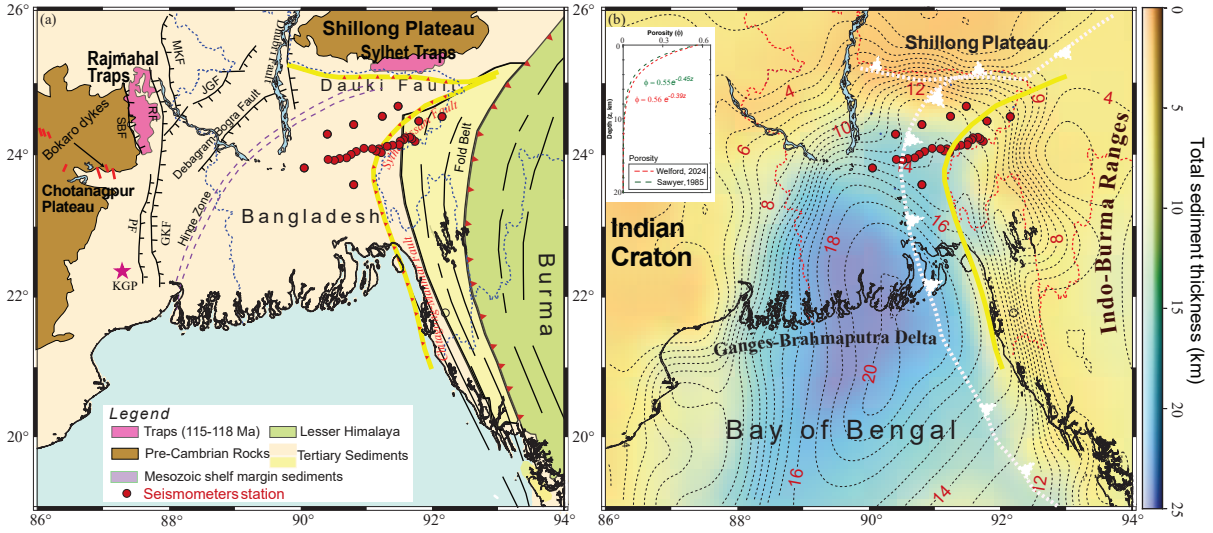
(a)
Shillong Plateau
Sylhet Traps
Rajmahal Traps
Dauki Fault
Bokaro dykes
Chotanagpur Plateau
Bangladesh
Burma
Fold Belt
Hinge Zone
KGP
MKF
JGF
IRF
SBF
GKF
PF
Legend
Traps (115-118 Ma)
Lesser Himalaya
Pre-Cambrian Rocks
Tertiary Sediments
Mesozoic shelf margin sediments
Seismometers station
(b)
Shillong Plateau
Indian Craton
Indo-Burma Ranges
Ganges-Brahmaputra Delta
Bay of Bengal
Porosity
Wellford, 2024
Sawyer, 1985
Total sediment thickness (km)
26°
24°
22°
20°
86°
88°
90°
92°
94°

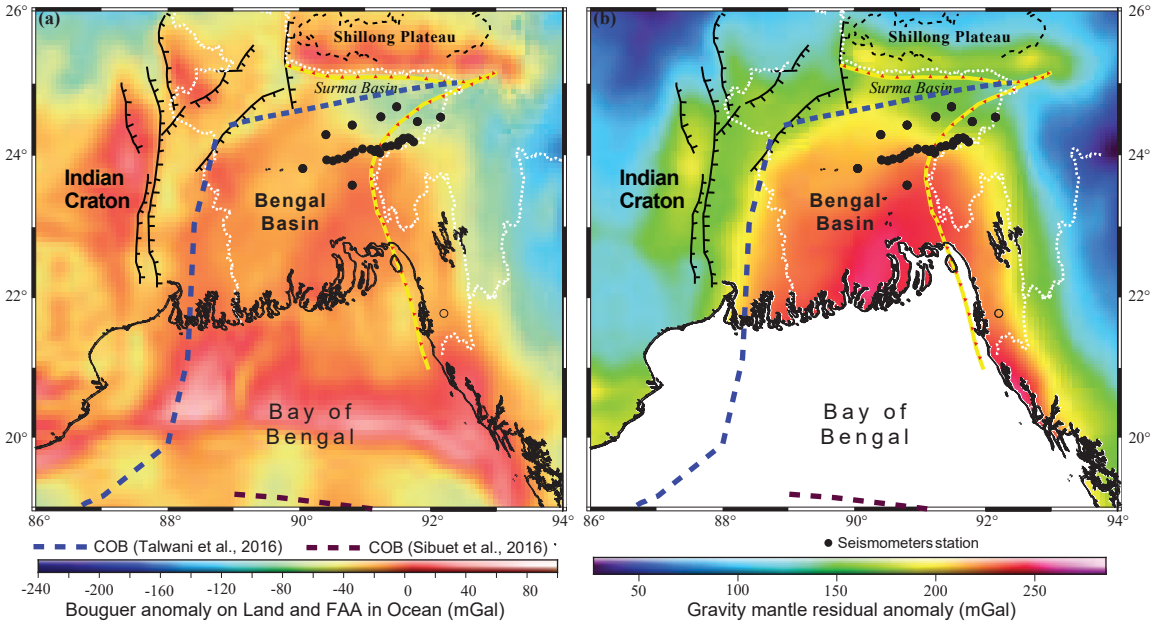
(a)
(b)
Shillong Plateau
Surma Basin
Indian Craton
Bengal Basin
Bay of Bengal
26°
24°
22°
20°
86°
88°
90°
92°
94°
COB (Talwani et al., 2016)
COB (Sibuet et al., 2016)
Seismometers station
-240
-200
-160
-120
-80
-40
0
40
80
Bouguer anomaly on Land and FAA in Ocean (mGal)
50
100
150
200
250
Gravity mantle residual anomaly (mGal)

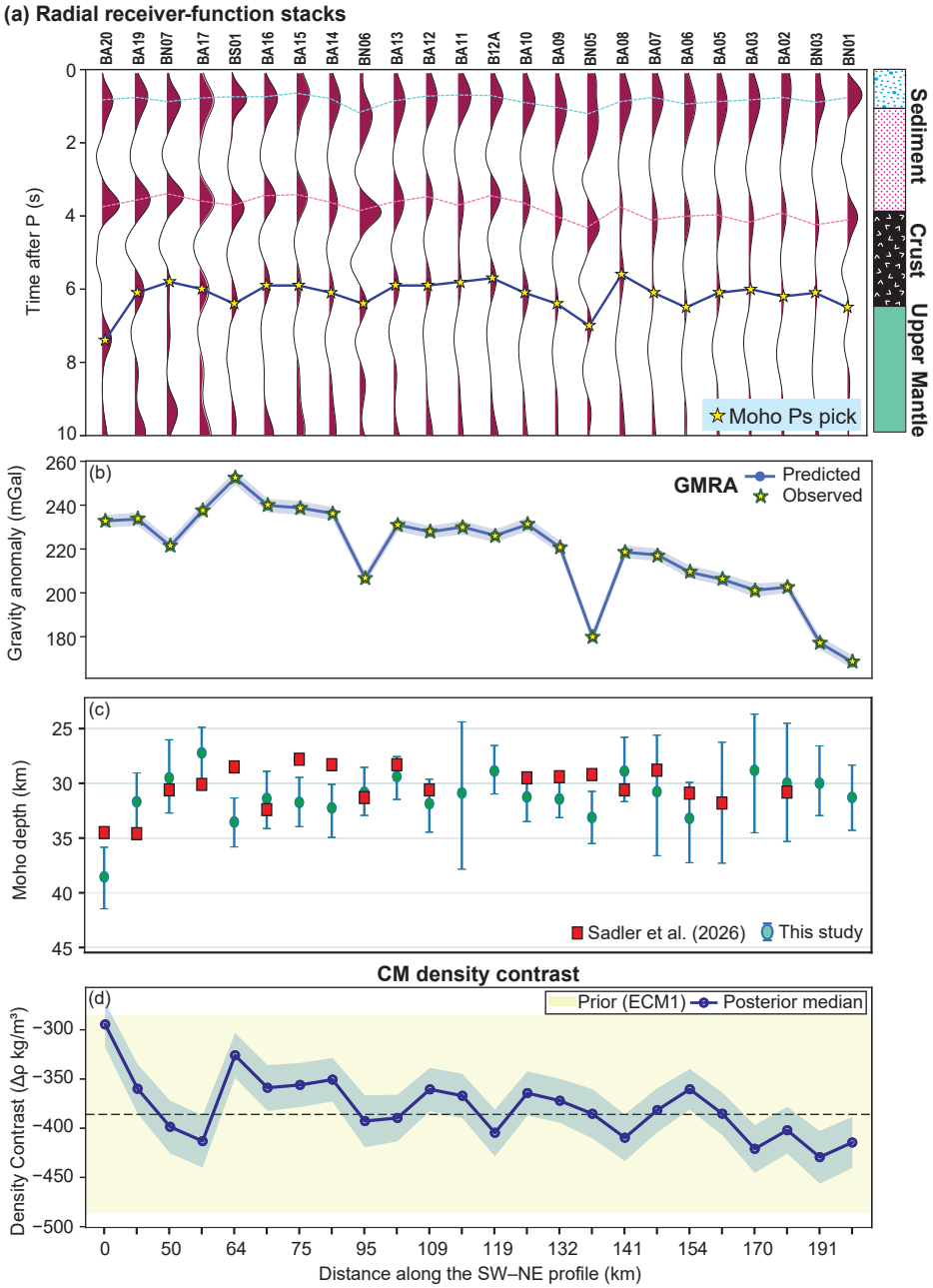
(a) Radial receiver-function stacks
BA20
BA19
BN07
BA17
BS01
BA16
BA15
BA14
BN06
BA13
BA12
BA11
B12A
BA10
BA09
BN05
BA08
BA07
BA06
BA05
BA03
BA02
BN03
BN01
Time after P (s)
Moho Ps pick
Sediment
Crust
Upper Mantle
(b)
GMRA
Predicted
Observed
Gravity anomaly (mGal)
(c)
Moho depth (km)
Sadler et al. (2026)
This study
CM density contrast
(d)
Prior (ECM1)
Posterior median
Density Contrast (Δρ kg/m³)
Distance along the SW–NE profile (km)

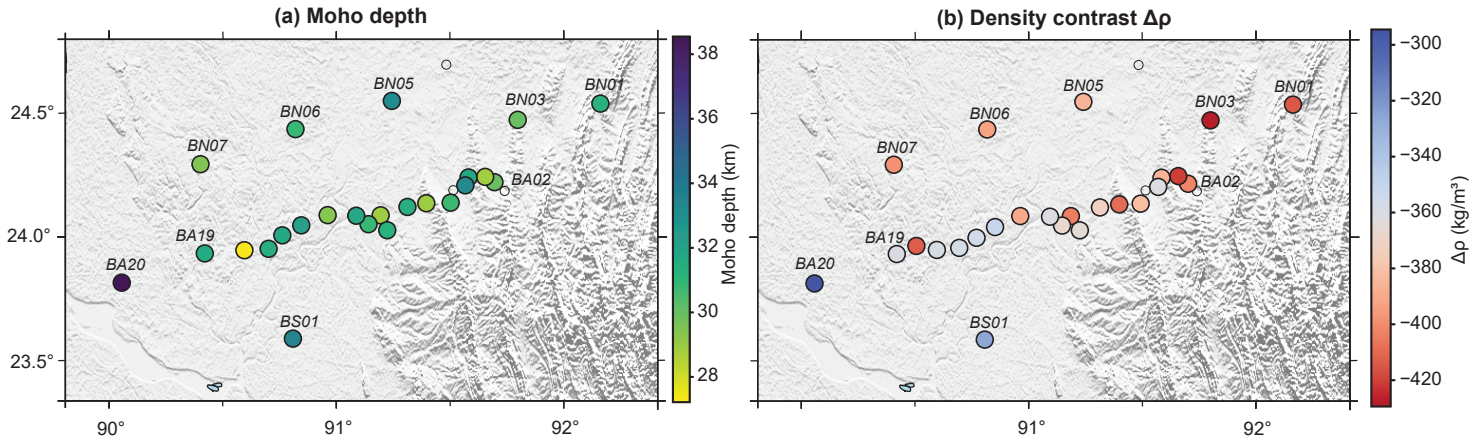
(a) Moho depth
BN01
BN03
BN05
BN06
BN07
BA02
BA19
BA20
BS01
24.5°
24.0°
23.5°
90°
91°
92°
38
36
34
32
30
28
Moho depth (km)
(b) Density contrast Δρ
−300
−320
−340
−360
−380
−400
−420
Δρ (kg/m³)

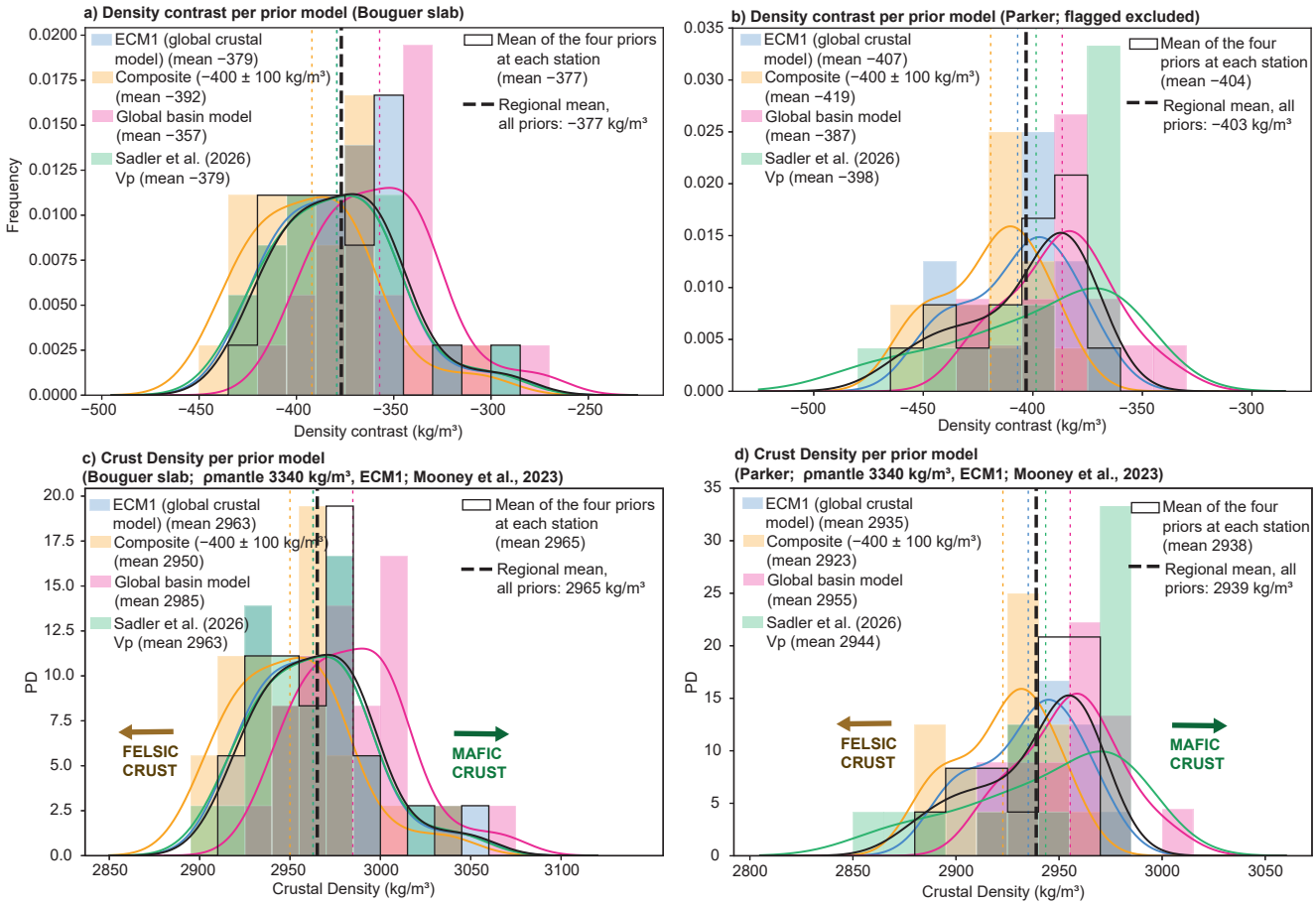
a) Density contrast per prior model (Bouguer slab)
ECM1 (global crustal model) (mean −379)
Composite (−400 ± 100 kg/m³) (mean −392)
Global basin model (mean −357)
Sadler et al. (2026) Vp (mean −379)
Mean of the four priors at each station (mean −377)
Regional mean, all priors: −377 kg/m³
Frequency
Density contrast (kg/m³)
b) Density contrast per prior model (Parker; flagged excluded)
ECM1 (global crustal model) (mean −407)
Composite (−400 ± 100 kg/m³) (mean −419)
Global basin model (mean −387)
Sadler et al. (2026) Vp (mean −398)
Mean of the four priors at each station (mean −404)
Regional mean, all priors: −403 kg/m³
Density contrast (kg/m³)
c) Crust Density per prior model (Bouguer slab; ρmantle 3340 kg/m³, ECM1; Mooney et al., 2023)
ECM1 (global crustal model) (mean 2963)
Composite (−400 ± 100 kg/m³) (mean 2950)
Global basin model (mean 2985)
Sadler et al. (2026) Vp (mean 2963)
Mean of the four priors at each station (mean 2965)
Regional mean, all priors: 2965 kg/m³
FELSIC CRUST
MAFIC CRUST
PD
Crustal Density (kg/m³)
d) Crust Density per prior model (Parker; ρmantle 3340 kg/m³, ECM1; Mooney et al., 2023)
ECM1 (global crustal model) (mean 2935)
Composite (−400 ± 100 kg/m³) (mean 2923)
Global basin model (mean 2955)
Sadler et al. (2026) Vp (mean 2944)
Mean of the four priors at each station (mean 2938)
Regional mean, all priors: 2939 kg/m³
FELSIC CRUST
MAFIC CRUST
PD
Crustal Density (kg/m³)

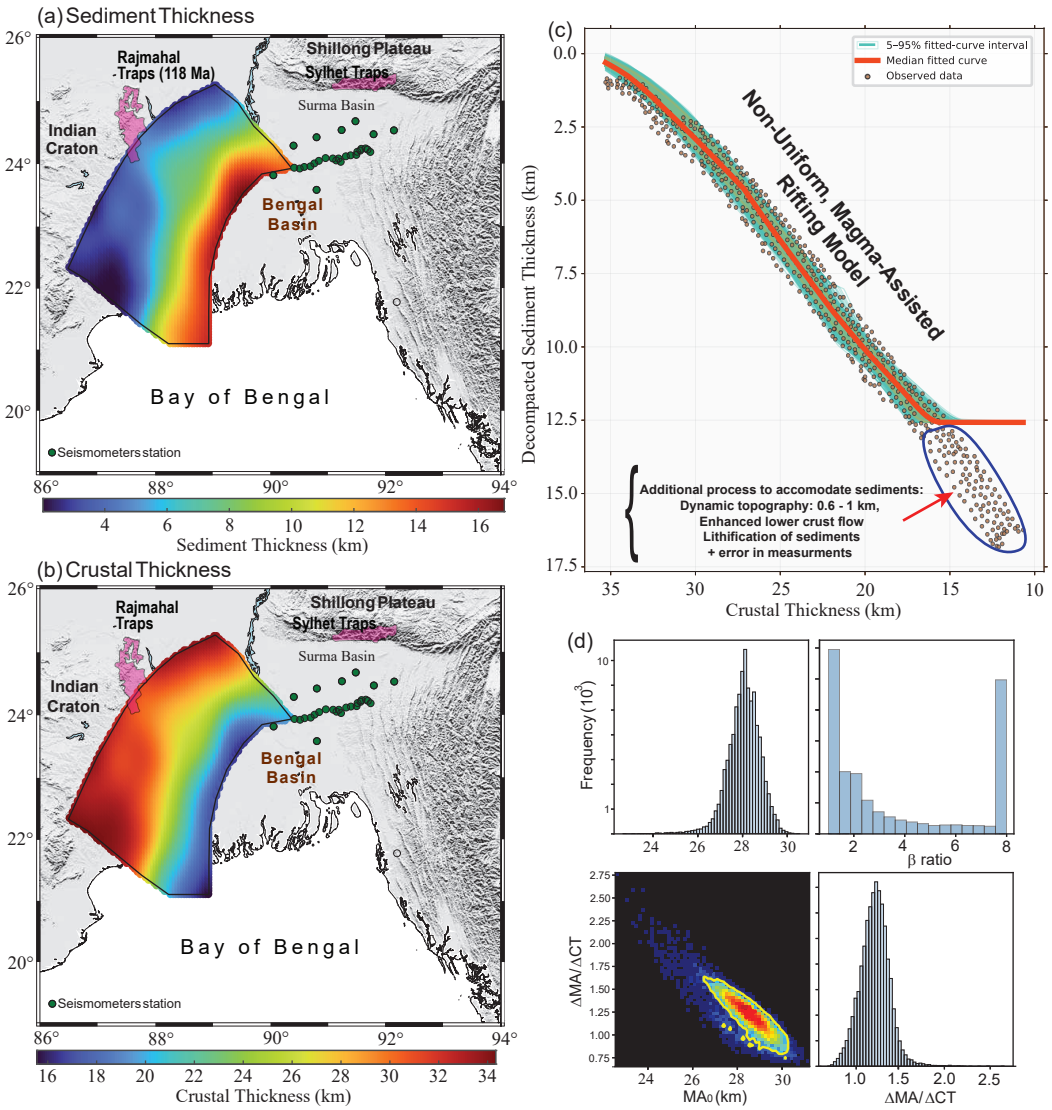
(a) Sediment Thickness
Rajmahal Traps (118 Ma)
Shillong Plateau
Sylhet Traps
Surma Basin
Indian Craton
Bengal Basin
Bay of Bengal
Seismometers station
Sediment Thickness (km)
(b) Crustal Thickness
Crustal Thickness (km)
(c)
5–95% fitted-curve interval
Median fitted curve
Observed data
Non-Uniform, Magma-Assisted Rifting Model
Decompacted Sediment Thickness (km)
Additional process to accomodate sediments:
Dynamic topography: 0.6 - 1 km,
Enhanced lower crust flow
Lithification of sediments
+ error in measurments
Crustal Thickness (km)
(d)
Frequency (10^3)
β ratio
ΔMA/ΔCT
MA0 (km)

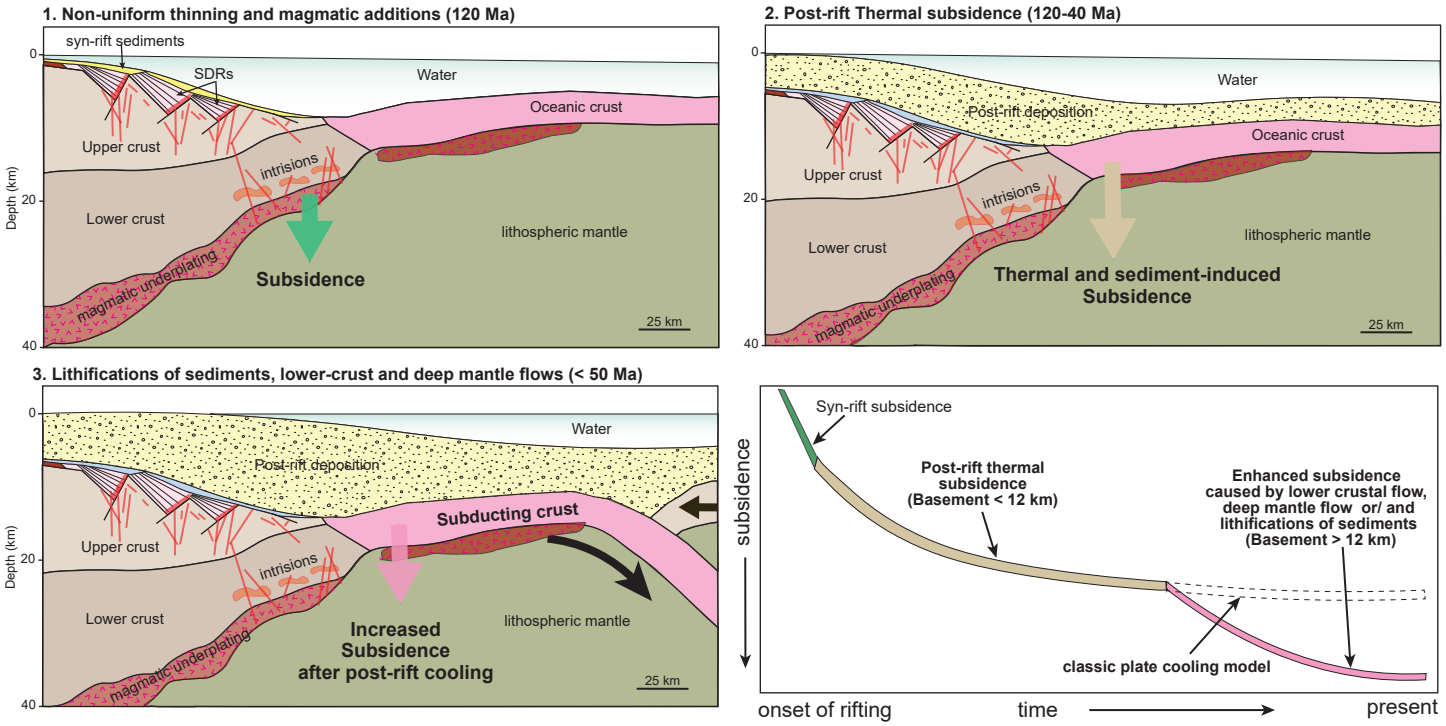
1. Non-uniform thinning and magmatic additions (120 Ma)
syn-rift sediments
SDRs
Water
Oceanic crust
Upper crust
intrisions
Lower crust
lithospheric mantle
magmatic underplating
Subsidence
25 km
Depth (km)
0
20
40
2. Post-rift Thermal subsidence (120-40 Ma)
Water
Post-rift deposition
Oceanic crust
Upper crust
intrisions
Lower crust
lithospheric mantle
magmatic underplating
Thermal and sediment-induced
Subsidence
25 km
3. Lithifications of sediments, lower-crust and deep mantle flows (< 50 Ma)
Water
Post-rift deposition
Subducting crust
Upper crust
intrisions
Lower crust
lithospheric mantle
magmatic underplating
Increased
Subsidence
after post-rift cooling
25 km
Syn-rift subsidence
Post-rift thermal
subsidence
(Basement < 12 km)
Enhanced subsidence
caused by lower crustal flow,
deep mantle flow or/ and
lithifications of sediments
(Basement > 12 km)
classic plate cooling model
subsidence
onset of rifting
time
present

Supplementary Files

This is a list of supplementary files associated with this preprint. Click to download.

- SupportingMaterials.docx